Utah State University
DigitalCommons@USU

All Physics Faculty Publications | Physics

2003

Secondary Electron Production and Transport Mechanisms by Measurement of Angle-EnergyResolved Cross Sections of Secondary and Backscattered Electrons

Jason Kite

JR Dennison
Utah State University

Follow this and additional works at: http://digitalcommons.usu.edu/physics_facpub

Part of the Physics Commons

Recommended Citation
Jason Kite with JRDennison, "Secondary Electron Production and Transport Mechanisms by Measurement of Angle-Energy Resolved Cross Sections of Secondary and Backscattered Electrons," 9th Rocky Mountain NASA Space Grant Consortium Symposium, Salt Lake City, UT, May 2003.

This Presentation is brought to you for free and open access by the Physics at DigitalCommons@USU. It has been accepted for inclusion in All Physics Faculty Publications by an authorized administrator of DigitalCommons@USU. For more information, please contact becky.thoms@usu.edu.

Jason Kite with J.R Dennison, "Secondary Electron Production and Transport Mechanisms by Measurement of Angle-Energy Resolved Cross Sections of Secondary and Backscattered Electrons," 9th Rocky Mountain NASA Space Grant Consortium Symposium, Salt Lake City, UT, May 2003.

ELECTRON EMISSION CROSS SECTIONS FROM A POLYCRYSTALLINE GOLD SURFACE

J.T. Kite, J.R. Dennison
Utah State University
Logan, UT 84321

Abstract

The angle dependence of emitted electron spectra from a polycrystalline Au surface has been measured at several incident electron beam energies. The range of incident energies (~100 eV to 2500 eV) extends from below the first crossover energy, through E_{max}, to above the second crossover energy. The traditional distinction between secondary electrons (<50 eV) and backscattered electrons (>50 eV) is found to be inconsistent with our energy- and angle-resolved measurements. We suggest a more "natural" delineation occurs at the local minima of the emission spectra; this feature is studied as a function of incident energy and emission angle. This work is also supported by the NASA Space Environments and Effects Program.

Introduction

Energetic primary electrons (PE's) incident on a surface induce electron emission from the surface. All of the emitted electrons, directly or indirectly, come from these incident PE's. Backscattered electrons (BSE's) originate from elastic or inelastic PE collisions within the solid. Secondary electrons (SE's) originate via interactions of PE's or BSE's with electrons in the solid (Fig. 1). Most SE's that leave the sample originate within a mean free path of their point of excitation, which is ~10-20 Å for metals [*Everhart and Chung, 1972*]. SE's are consequently very sensitive to surface conditions, composition, and crystal structure. The specific interactions that take place to produce BSE's and SE's can be investigated by studying the energy and angular resolved (ER and AR) distributions of all the electrons emitted from the surface [*Davies, 1999*]. In fact, the leading theorists in the field state that, "The maximum information about the SE emission process can be obtained by measuring the number of SE's emitted per second from 1 cm^2 of the surface with energy E in the direction Ω." [Rösler and Brauer, *1981*]

Measured SE's are conventionally defined to have energies below 50 eV, though doubt has been cast on this arbitrary definition [*Davies, 1999, p. 164*]. BSE's, believed to interact through combinations of elastic and inelastic collisions with the material, make up the rest of the electrons with energies greater than 50 eV. A typical energy resolved spectra shows the differentiated ratio of incoming to outgoing current flows versus negative potential detector bias (Fig. 2).

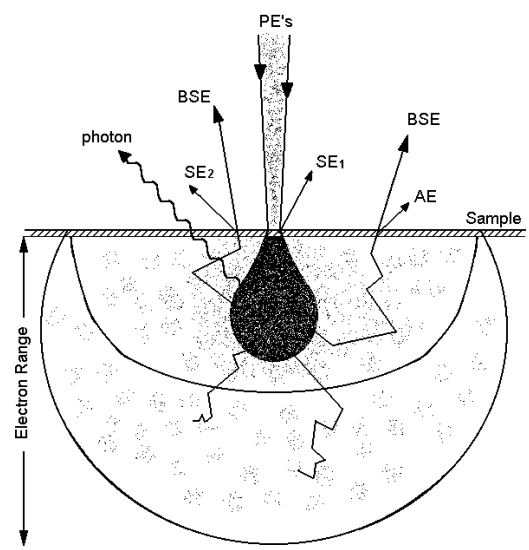

Figure 1. Physical processes resulting from energetic electron bombardment of a surface. Backscattered electrons (BSE), secondary electrons (SE_1) produced by primary electrons (PE), secondary electrons (SE_2) produced by BSE, Auger electrons (AE), and photons produced through inverse photoemission are shown. The hatched area shows the depth of predominant SE production [*Reimer, 1993*]. The shading shows the magnitude of the electron density.

Applications of SE and BSE emission

The general study of SE/BSE emission has many important applications. Three important charging phenomena directly related to SE emission are: (**i**) the detrimental effects associated with spacecraft charging and their applications [*DeForest, 1972; Froonincks, 1992; Katz, 1986; Garrett, 1987, 1989; Hastings, 1998; Wipple 1981; Davies 1996; Nickles, 1999; Chang, 2000*], (**ii**) the effects of high-voltage arcing and "snapover" [*Mandell, 1985; Hastings, 1989; Davies, 1997; Thompson,*

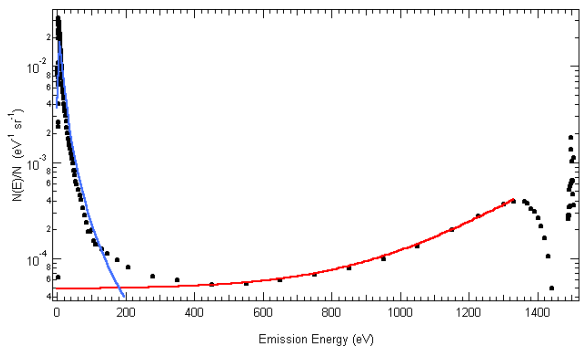

Figure 2. AR spectrum with log scale electron count vs. negative detector bias (emission energy). Primary energy of 1.5 keV at normal incidence on polycrystalline Au sample D6 at a 17° emission [*Davies, 1999*]. Blue line is Chung and Everhart Fit. Red line is empirical exponential fit.

2000], and (**iii**) plasma-induced small-particle charging [*Chow, 1993*]. There are also three technological advances currently being studied that are directly related to SE emission: (**i**) improved understanding and development of the electron microscope [*Seiler, 1983; Reimer, 1986, 1993*], (**ii**) electron-emission sources for the development of electron multipliers and flat-panel displays [*Kumar, 1995*], and (**iii**) plasma limiters deposited at the walls of nuclear fusion plasma devices [*Farhang, 1993*].

Importance of SE production mechanisms

The process through which a SE is produced can be modeled as three successive stages: the creation of the SE in the bulk, the transport of the SE from the point of creation to the surface, and the emission of the SE from the surface. The vast majority of theoretical work has involved modeling SE emission with a standard semi-empirical theory developed by Salow and Bruining [*Dionne, 1973*] using an expression for the number of SE's produced per PE (or SE Yield, δ)

$$\boldsymbol{\delta} = \int (-dE/dx)\, B\, e^{-\lambda x}\, dx. \qquad (1)$$

Each of these three stages corresponds to a measured parameter. The "stopping power", -(dE/dx), describes the energy transferred from the PE to the SE at a depth x; the inverse mean-free-path, λ, parameterizes the SE transport to the surface; and the constant B is the probability that a SE escapes the surface. Improvements to the theory by Baroody [*1950*], Sternglass [*1950,1957*], Barut [*1954*], Lye and Dekker [*1957*], and Dionne [*1975*] have incorporated slightly different assumptions for the energy loss term, E(x). For example, Sternglass uses the Bethe stopping power formula $(dE/dx) = F \cdot E^{-1} \ln(E/I)$, where F and I are material dependent factors [*Kanter, 1961; Suszcynsky and Borovsky, 1992*]. Alternately, other semi-empirical theories [*Schou, 1988; Reimer, 1993*] model the stopping power in terms of a power law formula of the form $dE/dx = A \square E^n$. All of these semi-empirical theory variations assume an isotropic angular distribution of SE production mechanisms and therefore successfully account for the low energy features in the AR spectra (e.g. Fig. 2). However, they are incomplete because they do not address SE creation mechanisms resulting from energy exchange within the solid.

Theory for SE Creation and Transport mechanisms

A quantum mechanical theory is needed to address these creation mechanisms as well as investigate whether the AR emission spectrum is indeed isotropic. In such theoretical treatments, the creation of the SE is addressed by considering three types of energy exchange within the solid: (**i**) the excitation of valence electrons, (**ii**) the excitation of core electrons, and (**iii**) the electron excitation due to plasmon decay [*Amelio, 1970; Powell and Woodruff, 1972*]. Knowing the probability for creating a secondary electron due to each of these energy exchange mechanisms allows one to calculate the transition probability between Bloch states. The resulting ER and AR distribution function for these distinct creation mechanisms (e.g. Fig. 3) can then be propagated to the surface using the Boltzmann transport equation [*Bindi, 1980*] or Monte Carlo techniques. The full development of the quantum mechanical theories [Ono, *1978*] have been derived and simulated by Rösler and Brauer [*1981*] and Ganachaud and Cailler [*1979*].

The result of the Rösler and Brauer calculation of the AR emission spectrum of aluminum is particularly interesting. They predicted isotropic (cosine) emission distributions for each mechanism as well as a combined total [see Fig. 4**(a)**] by adding the different SE excitation mechanisms (Fig. 3). Ganachaud and Cailler also predicted an isotropic total emission distribution in the Al cross sections [see Fig. 4**(b)**] using their unique **randium** (random ion position) and **jellium** (free electron gas) model.

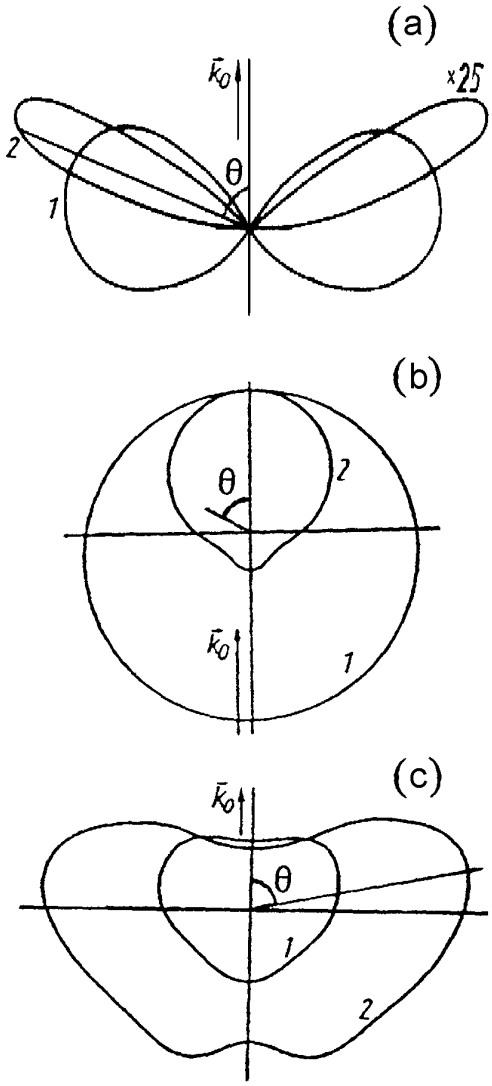

Figure 3. Angular dependence of excitation **(a)** by dynamical screened electron-electron scattering with a secondary electron energy of (1) 20 eV and (2) 200 eV **(b)** by core electron excitations with a secondary electron energy of (1) 50 eV and (2) 200 eV and **(c)** by plasmon decay with a secondary electron energy of (1) 20 eV and (2) 26 eV. Primary energy of 2 keV in aluminum [*Rösler and Brauer, 1981*].

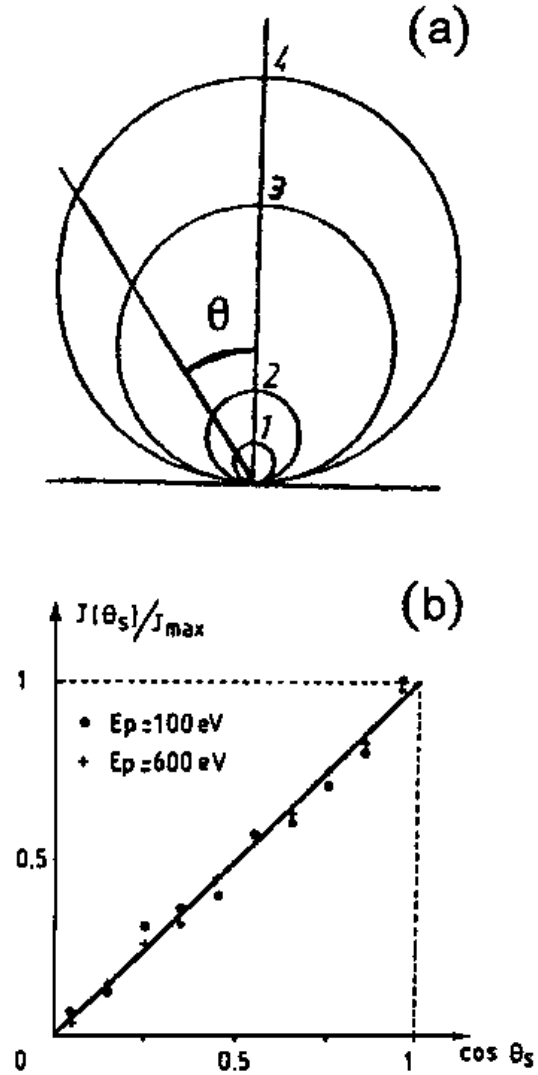

Figure 4. AR electron emission distributions **(a)** at 2 eV emission energy for 2 keV PE's normally incident on polycrystalline Al. Contributions are from different excitation mechanisms (1) core electrons, (2) electron-electron, (3) plasmon decay, and (4) combined total. [*Rösler and Brauer, 1981*]. **(b)** at 0 - 50 eV emission energy for 100 eV and 600 eV PE's normally incident on polycrystalline Al [*Ganachaud and Cailler, 1979*]. • and + data are also shown [*Jonker, 1951; Jahrreiss and Oppel, 1972*]. Line is cosine law.

In contrast to the theory, highly anisotropic angle dependent excitation distributions were found for the SE's excited by the three creation mechanisms on gold. (Figs. 5 and 6) This material was chosen because some fine structure has been found. The important result of these quantum mechanical SE theories relevant to this study is the prediction of highly anisotropic excitation distributions becoming isotropic during transport to the surface where emission takes place.

As an aside, there is great interest in aluminum because much fine structure exists due to the strong electron-plasmon coupling (or energy exchange) in the material [*Henrich, 1973*]. Ganachaud and Cailler note that, "For Al, the characteristic loss spectra show peaks corresponding to the creation of one or several successive bulk plasmons (up to 10)." There has been much theoretical argument as to whether any other nearly-free-electron (NFE) metals have electron-plasmon coupling [*Henrich, 1973*].

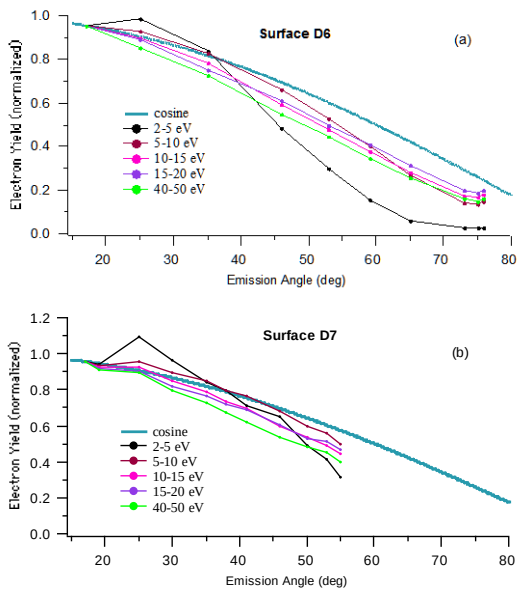

Figure 5. SE cross sections for the energy resolutions 2-5 eV, 5-10 eV, 10-15 eV, 15-20 eV, and 40-50 eV on polycrystalline Au (**a**) surface D6 and (**b**) surface D7 with PE energy of 1500 eV at normal incidence. Cosine curve is shown in blue. [*Davies, 1999, p. 157*]

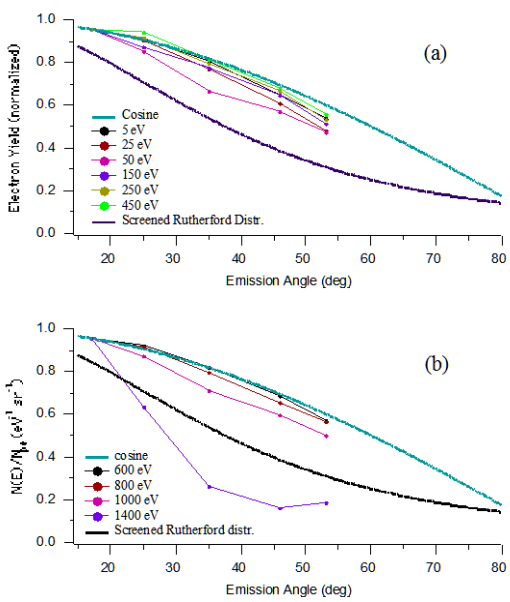

Figure 6. Selected ER cross sections with PE energy of 1500 eV at normal incidence on polycrystalline Au sample D6 (**a**) 5 eV, 25 eV, 50 eV, 150 eV, 250 eV, 450 eV, (**b**) 600 eV, 800 eV, 1000 eV, 1400 eV. Cosine curve is shown in blue. [*Davies, 1999, p. 160,162*].

Experimental evidence has shown that there are other NFE metals, which have electron-plasmon coupling [*Amelio, 1970*; *Haque and Kliewer, 1973*]. For example, Chung and Everhart state, "Low-q plasmon decay plays an important role in SE emission, which is not restricted to Al alone but should be valid in other NFE metals as well." [*1976, p. 4712*] Regardless of the implicit interest in electron-plasmon coupling, other NFE metals have creation mechanisms similar to Al in that they are highly anisotropic.

Since the inelastic mean free path for NFE metals is approximately the same, the transport mechanism should also be similar. Therefore, it is reasonable to infer an isotropic total emission distribution for the AR SE cross sections of NFE metals. Au is the only NFE material that does not oxidize and would therefore be a candidate as a standard.

Experimental Setup

A UHV (10^{-11} torr) chamber has already been built at Utah State University with a pristine sample environment for these ER AR scattering measurements. Periodic Ar sputtering and annealing of the Au sample confirms uniform, polycrystalline ordering. Magnetic fields have been measured at <10 mGauss and ambient electric fields have been measured by utilizing the rotatable retarding field analyzer Faraday cup detector (RD) angle symmetry placement. The RD has energy resolution of 0.3 eV and angluar resolution of 2°. Low incident beam currents (10 to 80 nA) have been used to minimize contamination effects [Dennison, 1997, Chang, 2000].

Integration Boundary for Yield Calculation

As seen in figure 2, there is clearly a sizable portion of SE's emitted with energy greater than 50 eV. The SE peak has been fit with the Chung and Everhart model and the BSE region with an imperical exponential fit. To account for the portion of miscounted SE's, a more reasonable choice of boundary, near the tail crossing of these fits, was used to calculate yields. The position, E_{min}, of the local minimum, N_{min}, between the SE and BSE regions has been measured for several different incident beam energies (Fig. 5). The reduced local minimum, E_{min}/E_{beam}, is also shown (Fig. 6). There is no noticeable angle dependence of E_{min}.

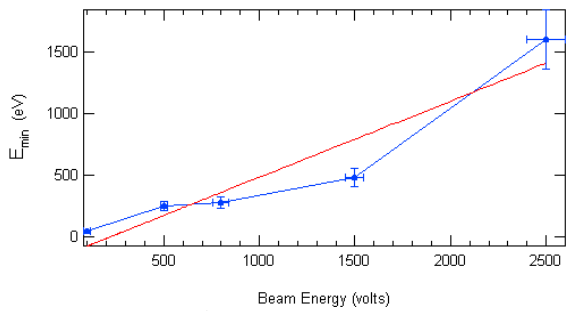

Figure 5. Position of the local minimum, E_{min} vs. incident beam energy at 45 degrees. A line fit is included in red.

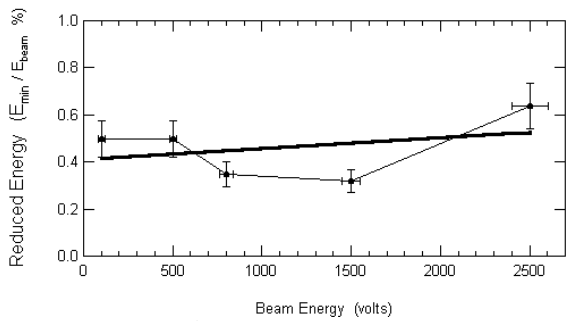

Figure 6. Position of the reduced local minimum, Emin/Ebeam vs. incident beam energy at 45 degrees. A line fit is included in black.

E_{min} was used as the integral boundary condition for calculating yields. The SE yield (0 to Emin) and BSE yield (Emin to Ebeam) were calculated for each distribution of AR spectra at beam energies of 500V, 900V, aand 2500V. The AR SE cross sections are shown in figure 7 and the AR BSE cross sections are shown in figure 8.

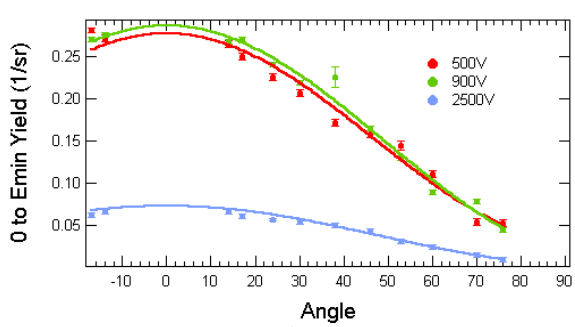

Figure 7. AR SE cross sections for 500V, 900V, and 2500V incident beam energys. Cosine fits are included.

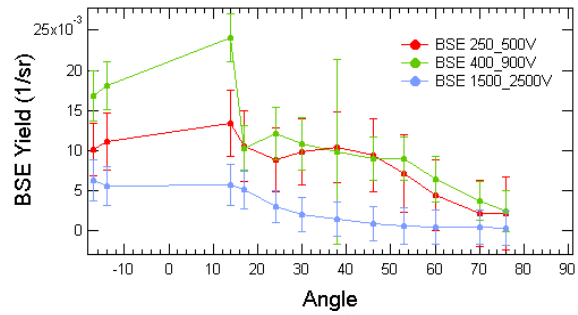

Figure 8. AR BSE cross sections for 500V, 900V, and 2500V incident beam energys.

Conclusion

In distinguishing SE's from BSE's, a clarification must be made about the subtle difference between excited (true) SE's and emitted (detected) SE's. Every emitted SE will be an excited SE, but not every excited SE will become an emitted SE. The use of the traditional 50 eV boundary condition leads to erroneous AR SE cross sections. However, use of the more natural delineation at the local minimum, E_{min}, as the boundary condition does lead to isotropic AR SE cross sections as theoretically predicted. Any deviations from isotropic AR SE cross sections can lead to new insight about the amounts of the three major types of excitation mechanism.

References

Amelio, G.F., Theory for the energy distribution of secondary electrons, *The Journal of Vacuum Sci. and Tech.*, *7*, *6*, 593-604, 1970.

Baroody, E.M., A theory of secondary electron emission from metals, *Phys. Rev.*, *78*, *6*, 780-787, 1950.

Barut, A.O., The mechanism of secondary electron emission, *Phys. Rev.*, *93*, *5*, 981-984, 1954.

Bindi, R., H. Lanteri and P. Rostaing, A new approach and resolution method of the Boltzmann equation applied to secondary electron emission, by reflection from polycrystalline aluminium, *J. Phys. D: Appl. Phys.*, *13*, 267-280, 1980.

Chang, W.Y., J. R. Dennison, Jason Kite, and R. E. Davies, Effects of evolving surface contamination of spacecraft charging, Proceedings of the 38th American Institute of Aeronautics and Astronomics on Aerospace Sciences, Paper received Certificate of Merit by the AIAA Plasmadynamics and Lasers

Technical Committee for Best Paper of 2000 (Reno, NV, 2000), in press.

Chow, V.W., D. A. Mendis and M. Rosenberg, Role of grain size and particle velocity distribution in secondary electron emission in space plasmas, *J. Geophys. Res., 98*, 19065, 1993.

Chung, M.S., and T.E. Everhart, Role of plasmon decay in secondary electron emission in the nearly-free-electron metals. Application to aluminum, *Phys. Rev. B, 15*, 10, 1977.

Davies, R.E., Measurement of Angle-Resolved Secondary Electron Spectra, Doctoral Dissertation, Dept. of Physics, Utah State Univ., Logan, UT, 1999.

Davies, R.E., and J.R. Dennison, Evolution of secondary electron emission characteristics of spacecraft surfaces, J. *Spacecraft Rockets*, 34, 4, 571-574, 1997.

Davies, R.E., An instrument for experimental secondary electron emission investigations, with application to the spacecraft charging problem, M.S. Thesis, 220 pp., May, 1996.

DeForest S.E, Spacecraft charging at synchronous orbit, *J. Geophys. Res., 77*, 651, 1972.

Dionne, G.F., Origin of secondary-electron-emission yield-curve parameters, *J. Appl. Phys., 46, 8*, 3347-3351, 1975.

Dionne, G.F., Effects of secondary electron scattering on secondary emission yield curves, *J. Appl. Phys., 44, 12*, 5361-5364, 1973.

Drescher, H., L. Reimer, and H. Seidel, Backscattering and secondary electron emission of 10-100 keV electrons and correlations to scanning electron microscopy, *Z. f. Angew. Physik, 29, 6*, 331-336, 1970.

Everhart, T.E., M.S. Chung, Idealized spatial emission distribution of secondary electrons, *J. Appl. Phys, 43, 9*, 3707-11, 1972.

Farhang, H, E. Napchan, B.H. Blott, Electron backscattering and secondary electron emission from carbon targets: comparison of experimental results with Monte Carlo simulations, *J. Phys. D: Appl. Phys, 26*, 2266-2271, 1993.

Frooninckz, T., J.J. Sojka, Solar cycle dependence of spacecraft charging in low earth orbit, *J. Geophys. Res., 97*, 29851, 1992.

Ganachaud, J.P., and M. Cailler, A monte-carlo calculation of the secondary electron emission of normal metals I. The model, *Surf. Sci., 83*, 498-518, 1979.

Ganachaud, J.P., and M. Cailler, A monte-carlo calculation of the secondary electron emission of normal metals II. Results for aluminum, *Surf. Sci., 83*, 519-530, 1979.

Garrett, H.B., The charging of spacecraft surfaces, *Rev. Geophys., 19*, 577, 1981.

Garrett, H.B., 1987.

Guinier, A.and R. Griffoul, *Compt. Rend., 221*, 555-557, 1945.

Hastings, D.E., P. Chang, The physics of positively biased conductors surrounded by dielectrics in contact with a plasma, *Phys. Fluids B, 1*, 1123, 1989.

Haque and Kliewer, Plasmon properties in bcc potassium and sodium, *Phys. Rev., B7*, 2416, 1973.

Henrich, V.E., Role of bulk and surface plasmon in the emission of slow secondary electrons: polycrystilline aluminum, Phys. Rev. B, 7, 8, 3512-19, 1973.

Jahrreiss, H., and W. Oppel, Angular distributions of secondary electrons originating from thin films of different metals in re-emission and transmission, *J. Vac. Sci. Tech., 9, 1*, 173-176, 1972.

Jonker, J.L.H., The angular distribution of the secondary electrons of nickel, *Philips Res. Rep. 6*, 372-387, 1951.

Kanter, H., Contribution of backscattered electrons to secondary electron formation, *Phys. Rev., 121, 3*, 681-684, 1961.

Katz, I., M. Mandel, G. Jongeward, M.S. Gussenhoven, The importance of accurate secondary electron yields in modeling spacecraft charging, *J. Geophys. Res., 91*, 13739, 1986.

Kumar, N., Diamond-based field emission flat panel displays, *Solid State* Technology, 71 May 1995.

Lye, R.B., and A.J. Dekker, Theory of secondary emission, *Phys. Rev., 107, 44*, 977-981, 1957.

Mandell, M.J., I. Katz, G.A. Jongeward, and J.C. Roberts, Computer simulation of plasma electron collection by PIX-II, J. *Spacecrafts and Rockets, 23*, 512, 1985.

Nickles, N., R.E. Davies, J.R. Dennison, Applications of secondary electron energy- and angular-distributions to spacecraft charging, 1999.

Ono, S. and K. Kanaya, The energy dependence of secondary emission based on the range-energy retardation power formula, *J. Phys. D: Appl. Phys*., 12, 619-632, 1979.

Powell, B.D., and D.P. Woodruff, Plasmon effects in electron energy loss and gain spectra in aluminum, *Surface Science, 33*, 437-444, 1972.

Reimer, L., Image Formation in low-voltage scanning electron microscopy, 144 pp., SPIE, Bellingham, WA, 1993.

Reimer, L., and D. Stelter, FORTRAN 77 Monte-Carlo program for minicomputers using Mott cross-sections, Scanning, 8, 265-277, 1986.

Rösler, M., and W. Brauer, Theory of secondary electron emission I. General theory for nearly-free-electron metals, *Phys. Stat. Sol. (b), 104*, 161 161-175, 1981a.

Rösler, M., and W. Brauer, Theory of secondary electron emission II. Application to aluminum, *Phys. Stat. Sol. (b), 104*, 575-587, 1981b.

Schou, J., Secondary electron emission from solids by electron and proton bombardment, *Scanning Microscopy, 2*, 2, 607-632, 1988.

Seiler, H., Secondary electron emission in the scanning electron microscope, *J. Appl. Phys., 54*, R1-R18, 1983.

Sternglass, E.J., Theory of secondary electron emission by high-speed ions, *Phys. Rev., 108, 1*, 1-12, 1957.

Sternglass, E.J., Secondary electron emission and atomic shell structure, *Phys. Rev., 80*, 925-926, 1950.

Suszcynsky, D.M., and J.E. Borovsky, Modified Sternglass theory for the emission of secondary electrons by fast-electron impact, *Phys. Rev. A, 45, 9*, 6424-6428, 1992.

Thompson, C.D., J.R. Dennison, R.E. Davies, D.C. Ferguson, J.T. Galafaro and B.V. Vayner, Investigation of the first snapover of positively biased conductors in a plasma, Proceedings of the 38th American Institute of Aeronautics and Astronomics on Aerospace Sciences, (Reno, NV, 2000), in press.

Wipple, E.C., Potentials of surfaces in space, *Rep. Prog. Phys., 44*, 1197, 1981.